EXAFS Comparison of the Dimanganese Core Structures of Manganese Catalase, Arginase, and Manganese-Substituted Ribonucleotide Reductase and Hemerythrin†

Timothy L. Stemmler,‡ Thomas M. Sossong, Jr.,§ Jonathan I. Goldstein,|| David E. Ash,*,§ Timothy E. Elgren,*,|| Donald M. Kurtz, Jr.,*,⊥ and James E. Penner-Hahn*,‡

Department of Chemistry, University of Michigan, Ann Arbor, Michigan 48109-1055, Department of Biochemistry, Temple University, Philadelphia, Pennsylvania 19140, Department of Chemistry, Hamilton College, Clinton, New York 13323, and Department of Chemistry and Center for Metalloenzyme Studies, University of Georgia, Athens, Georgia 30602

Received February 6, 1997; Revised Manuscript Received June 5, 1997⊗

ABSTRACT: The solution structures of the binuclear Mn centers in arginase, Mn catalase, and the Mn-substituted forms of the Fe enzymes ribonucleotide reductase and hemerythrin have been determined using X-ray absorption spectroscopy (XAS). X-ray absorption near edge structure (XANES) spectra for these proteins were compared to those obtained for Mn(II) models. The Mn model spectra show an inverse correlation between the XANES peak maximum and the root-mean-square (RMS) deviation in metal−ligand bond lengths. For these complexes, the XANES maxima appear to be more effective than the 1s → 3d areas as an indicator of metal-site symmetry. Arginase and Mn-substituted ribonucleotide reductase have symmetric nearest neighbor environments with low RMS deviation in bond length, while Mn catalase and Mn-substituted hemerythrin appear to have a larger RMS bond length deviation. The 1s → 3d areas for arginase and Mn-substituted ribonucleotide reductase are consistent with six coordinate Mn, while the 1s → 3d areas for Mn catalase and Mn-substituted hemerythrin are larger, suggesting that one or both of the Mn ions are five-coordinate in these proteins. Extended x-ray absorption fine structure (EXAFS) spectra were used to determine the Mn_2 core structure for the four proteins. In order to quantitate the number of histidine residues bound to the Mn_2 centers, EXAFS data for the crystallographically characterized model hexakis−imidazole Mn(II) dichloride tetrahydrate were used to calibrate the Mn−imidazole multiple scattering interactions. These calibrated parameters allowed the outer shell EXAFS to be fit to give a lower limit on the number of bound histidine residues. The EXAFS spectra for Mn-substituted ribonucleotide reductase and arginase are nearly identical, with symmetric Mn−nearest neighbor environments and outer shell scattering consistent with a lower limit of one histidine per Mn_2 core. In contrast, the EXAFS data for Mn catalase and Mn-substituted hemerythrin show two distinct Mn−nearest neighbor shells, modeled as Mn−O at ca. 2.1 Å and Mn−N at ca. 2.3 Å, and outer shell carbon scattering consistent with a lower limit of ca. 2−3 His residues per Mn_2 core. Only Mn catalase shows clear evidence for Mn···Mn scattering. The observed Mn···Mn distance is 3.53 Å, which is significantly longer than the ∼3.3 Å distances that are typically observed for $Mn(II)_2$ cores with two single atom bridges, but which is typical of the distances seen in $Mn(II)_2$ cores having one single atom bridge (e.g., aqua or hydroxo) together with one or two carboxylate bridges. The absence of EXAFS-detectable Mn···Mn interactions for the other three proteins suggests either that there are no single atom bridges in these cases or that the Mn···Mn interactions are more disordered.

Binuclear metal centers are utilized at the active sites of numerous iron and manganese metalloproteins. These proteins catalyze a diverse set of chemical reactions while maintaining structural and electronic similarities. Three such proteins which are believed to have similar active site structures are the diiron proteins hemerythrin and ribonucleotide reductase and the dimanganese protein Mn catalase (Kono & Fridovich, 1983; Barynin & Grebenko, 1986; Que & True, 1990; Stenkamp, 1994; Nordlund & Eklund, 1995). All three proteins have a carboxylate-bridged binuclear metal site bound within a four helix bundle (Petersson et al., 1980; Vainshtein et al., 1984; Khangulov et al., 1986; Fronko et al., 1988; Baldwin, 1990; Nordlund et al., 1990; Nordlund & Eklund, 1993, 1995; Stenkamp, 1994). Although it has a distinct secondary structure, rat liver arginase has a similar binuclear Mn site (Kanyo et al., 1996).

Hemerythrin and ribonucleotide reductase are binuclear iron proteins which perform oxygen transport and catalyze the conversion of nucleoside diphosphates to deoxynucleoside diphosphates, respectively (Kurtz et al., 1977; Stubbe & van der Donk, 1995). Manganese-substituted forms of both proteins have been prepared (Atta et al., 1992; Zhang & Kurtz, 1992). The crystal structure of Mn-substituted ribonucleotide reductase has a bis(μ-carboxylato) bridged Mn_2 core (Atta et al., 1992). In addition to the two bridging

† This work was supported in part by grants from the NIH [GM-45205 to J.P.H.; DK-44841 to D.E.A.; GM-40388 to D.M.K.; and the Howard Hughes Medical Institute (T.E.E.)]. SSRL and NSLS are supported by the U.S. Department of Energy with additional support from the NIH Research Resource program. Beamline X-19A was supported in part by the University of Michigan Office of the Vice President for Research.

* Authors to whom correspondence should be addressed.
‡ University of Michigan.
§ Temple University.
|| Hamilton College.
⊥ University of Georgia.

⊗ Abstract published in *Advance ACS Abstracts,* July 15, 1997.

S0006-2960(97)00279-1 CCC: $14.00

Scheme 1

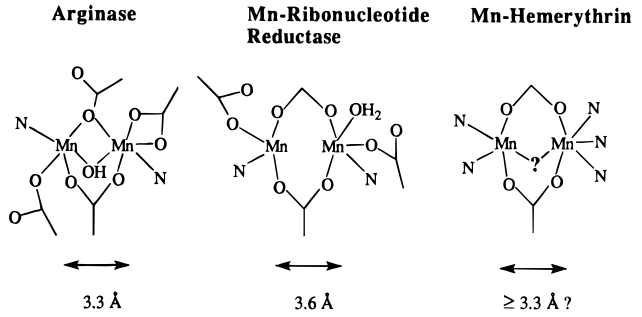

glutamates, the crystal structure shows the Mn ions to be coordinated to two histidines (one to each Mn), monodentate aspartate and glutamate residues, and one water molecule, thus completing four- and five-coordinate Mn(II) first coordination spheres. The Mn···Mn distance in the Mn-substituted ribonucleotide reductase crystal structure is 3.6 Å. The X-ray structure of the Mn-substituted form of hemerythrin has not been determined. However, the crystal structure of the native diiron(II) form, which should be generally similar, shows one five- and one six-coordinate Fe(II) in a bis(μ-carboxylato)(μ-hydroxo)diiron(II) core with five terminal histidine ligands and an Fe···Fe distance of 3.32 Å (Holmes et al., 1991). XAS studies of the Co-substituted form of hemerythrin indicate that this overall structure is maintained upon metal substitution, although the Co···Co distance increases to 3.54 Å (Zhang et al., 1992; Stenkamp, 1994).

The native forms of arginase and Mn catalase contain binuclear Mn active sites. These enzymes catalyze the hydrolysis of arginine and the disproportionation of hydrogen peroxide, respectively (Hertzfeld & Raper, 1976; Beyer & Fridovich, 1985; Kang & Cho, 1990). Arginase is found specifically in the Mn(II)/Mn(II) form, although the extent to which higher metal oxidation states are produced during catalysis is unknown (Greenberg, 1960; Reczkowski & Ash, 1992).

After completion of this work, the 2.1 Å crystal structure of arginase was reported (Kanyo et al., 1996). In this structure, the Mn ions are bridged by a solvent molecule, a μ-1,1-carboxylate and a μ-1,3-carboxylate, giving a Mn···Mn separation of 3.3 Å. The Mn coordination spheres are completed by one monodentate carboxylate, one bidentate carboxylate, and two histidines, giving one five- and one six-coordinate Mn. The metal ligation for arginase, Mn-ribonucleotide reductase, and hemerythrin are shown in Scheme 1, with the hemerythrin structure based on the crystal structure of ferrous hemerythrin.

In contrast to the other three proteins, Mn catalase can be prepared in a variety of oxidation states, ranging from Mn(II)/Mn(II) to Mn(III)/Mn(IV) (Khangulov et al., 1986, 1993; Fronko et al., 1988; Waldo, 1991). During catalysis, Mn catalase is believed to cycle between the Mn(II)/Mn(II) and Mn(III)/Mn(III) oxidation states (Waldo & Penner-Hahn, 1995). Analysis of EPR spectra for arginase and the Mn(II)/Mn(II)-phosphate derivative of *Thermus thermophilus* Mn catalase gave Mn−Mn separations of 3.57 and 3.59 Å, respectively (Khangulov et al., 1995). XAS, pulsed EPR, and MCD studies of the *Lactobacillus plantarum* and *T. thermophilus* Mn catalases suggest that the Mn is ligated predominately by oxygen ligands, with one or more nitrogen ligands (Waldo et al., 1992; Khangulov et al., 1993; Gamelin et al., 1994; Ivancich et al., 1995; Grush et al., 1996)

Arginase and Mn-substituted ribonucleotide reductase both catalyze hydrogen peroxide disproportionation (T. E. Elgren, unpublished results; Shank et al., 1994; Sossong et al., 1997), but at rates which are roughly 1000 times slower than that for Mn catalase. No reactivity toward H_2O_2 has been reported for Mn-substituted hemerythrin.

With the availability of a high-resolution crystal structure for Mn-substituted ribonucleotide reductase and, during this study, arginase, the immediate ligation of the Mn in these proteins is well-defined. In order to compare the Mn environment of Mn catalase to that of the Mn in the other proteins and to determine Mn−ligand distances for all four proteins with greater precision than is possible crystallographically, we have undertaken XAS studies. XAS, by permitting comparison of the Mn(II)/Mn(II) core structures in arginase, Mn catalase, and the Mn-substituted forms of hemerythrin and ribonucleotide reductase, will help to determine the structural constraints which control reactivity.

EXPERIMENTAL SECTION

Sample Preparation. Mn-substituted Fe ribonucleotide reductase was prepared as follows. R2 was isolated from *Escherichia coli* strain N6405/pSPS2, (Salowe & Stubbe, 1986) a heat-inducible overproducer, as previously described (Salowe, 1987). Iron removal was accomplished by dialysis against the lithium salt of 8-hydroxyquinoline-5-sulfonic acid in 1.0 M imidazole (Atkin et al., 1973). The concentration of $R2_{apo}$ was determined by absorbance at 280 nm (ϵ_{280} = 120 mM^{-1} cm^{-1}) (Lynch et al., 1989). Anaerobic addition of a Mn(II) solution [$MnCl_2 \cdot 4H_2O$ (J. T. Baker Chemical Co.)] to $R2_{apo}$ was accomplished using standard vacuum line techniques. The Mn-R2 sample was passed down a Sephadex G-25 column to remove any unbound metal ions. Samples prepared for XAS contained 4.5 equiv of Mn per R2 subunit, as determined by inductively coupled plasma emission, in 25 mM HEPES, pH 7.6.

Rat liver arginase was expressed in *E. coli* and purified as described by Cavalli et al. (1994). Ammonium sulfate precipitates of the enzyme were centrifuged, resuspended in 50 mM K^+-HEPES at pH 7.5 containing 10 mM $MnCl_2$, and heated to 60 °C for 10 min (Reczkowski & Ash, 1992). The protein samples were then washed four times with 50 mM K^+-HEPES at pH 7.5 in an Amicon Centricon-30 microconcentrator to remove unbound Mn(II) and concentrated to 50−90 mg/mL. Glycerol was added to the protein samples to a final concentration of 25%. Mn-substituted hemerythrin was prepared as previously described (Zhang, 1992; Zhang & Kurtz, 1992). Mn catalase was isolated from *L. plantarum* according to established methods (Kono & Fridovich, 1983; Stemmler, 1996). Samples of the reduced, Mn(II)/Mn(II), catalase were prepared by anaerobic reduction with NH_2OH (Waldo et al., 1991). All protein samples were prepared at Mn concentrations between 3 and 5 mM Mn and at a glycerol concentration of 25−50%. Protein solution samples were injected into Lucite cells wrapped with 30 μm polypropylene film, and immediately frozen at 77 K.

A solution sample of hexaqua Mn(II) (**A**) was prepared by dissolving Mn(II)$(acetate)_2$ (Aldrich) in water, adjusting the pH to 3.0 using nitric acid, and injecting the solution

with a Mn concentration of 10 mM into an Al sample cell wrapped with 30 μm polypropylene film. All other model complexes, which were generously provided by the Pecoraro, Kitajima, and Goff groups, were ground and mixed to homogeneity with boron nitride using a mortar and pestle, and then loaded into a 1 mm thick Al sample cell with Kapton windows. The solid mono-, di-, and tetranuclear Mn(II) model complexes, hexakis−imidazole Mn(II) dichloride tetrahydrate (**B**) (Garrett et al., 1983), $[Mn_3(Cl)_3(C_{42}H_{56}N_{12}](ClO_4)_3$ (**C**) (Goff, personal communication), (pyrazole)$_2$Mn(benzoate)$_3$Mn(hydrotris(3,5-diisopropyl-1-pyrazolyl)borate) (**D**) (Kitajima, personal communication), [Mn(*N*,*N*′-[1,1′-dithiobis(phenylene)]bis(salicylideneaminato))]$_2$ (**E**) (Kessissoglou et al., 1987), [Mn$_2$(2-OH(3,5-Cl(1,3-salcylideneimino-2-propanol)))$_2$](tetraethylamommium)$_2$ (**F**), (Gelasco, 1995) [Mn(hydrotris(3,5-diisopropyl-1-pyrazolyl)borate)$_3$]$_2$(OH)$_2$ (**G**) (Kitajima et al., 1991), and [Mn(2-OH(*N*,*N*′-(bis-1,3-(picolinimine(propan-2-ol)))))]$_4$ (**H**) (Gelasco et al., 1996), were prepared according to published procedures. After preparation, all model samples were frozen at 77 K.

XAS Collection and Analysis. Protein and model XAS spectra were collected at the Stanford Synchrotron Radiation Laboratory (SSRL), on beamlines II-3 and VII-3, and at the National Synchrotron Light Source (NSLS), at beamlines X9-A and X19-A. Both facilities were operating under dedicated conditions, with typical ring energies and currents of 3.0 GeV/100 mA and 2.5 GeV/200 mA for SSRL and NSLS, respectively. Details for the data collection and analysis of the Mn(II)/Mn(II) proteins and Mn(II) models are given in Table S1 (Supporting Information). Low temperatures were maintained using a He flow cryostat at beamlines II-3, VII-3, and X19-A, while a Dysplex cryostat was used at X9-A. XAS spectra were averaged independently for each data set collected at each location, with typical protein data sets consisting of 9−12 spectra and model data sets consisting of 2 or 3 spectra. Data for the proteins and for model **A** were measured as fluorescence excitation spectra using a 13 element solid state detector, while data for solid model compounds **B**−**H** were measured as absorption spectra using N_2 ion chambers. Monochromator energies were calibrated relative to the energy of the pre-edge peak in a $KMnO_4$ standard, defined as 6543.3 eV. Averaged EXAFS files were calculated using two data sets collected with different Mn-substituted ribonucleotide reductase samples (labeled Mn_2RR-1 and Mn_2RR-2 in Table 1), three EXAFS data sets for different arginase samples (Arg-1, Arg-2, and Arg-3), and three EXAFS data sets for the reduced Mn catalase (Cat-1, Cat-2, and Cat-3). Only a single data set was measured for Mn-substituted hemerythrin (Mn_2Hem).

Normalized XANES spectra were calculated for each data set by fitting the data both below and above the edge to tabulated X-ray absorption cross-sections, (McMaster et al., 1969; Waldo, 1991) using a single low-order polynomial and a single scale factor. Edge energies for all XANES spectra were taken as the first inflection point of the edge, determined from the maximum in the first derivative. First derivatives were calculated by differentiation of a running first-order polynomial, fit over a 30-point window. Areas for the 1s → 3d pre-edge transitions were determined by first fitting an arctangent background to the normalized data below and above the 1s → 3d transition. For Si[220], Si[311], and Si[400] monochromator crystals, fits were done over the range 6530−6538 eV and 6543−6545 eV. Due to the lower energy resolution for the Si[111] monochromator crystals, the 1s → 3d transitions measured using these monochromators were significantly broader. As a result, arctangent regions below (6530−6537 eV) and above (6544−6546 eV) the 1s → 3d transition were used for these data sets. The 1s → 3d area was determined by numerical integration over the range of 6538−6543 eV (Si[220], Si[311] and Si[400] data sets) or 6537−6544 eV (Si[111] data sets). The resulting 1s → 3d areas are expressed in electronvolt units (Roe et al., 1984).

Table 1: XANES Analysis Results for Mn(II) Protein (Top) and Model (Bottom) Samples with Relevant Model Mn First Coordination Sphere Ligand Types and Distance Information from Crystal Structure Data

sample	ligation	RMS deviation[a]	edge energy[b]	peak maxima[c]	1s → 3d area[d]
Mn_2RR-1			6549.2	780	7.20
Mn_2RR-2			6548.7	790	7.80
Arg-1			6549.1	810	7.40
Arg-2			6549.0	800	7.50
Arg-3			6549.5	800	7.60
Cat-1			6549.0	660	10.0
Cat-2			6548.4	660	10.7
Cat-3			6549.2	670	11.1
Mn_2Hem			6548.0	710	12.3
A	O_6		6549.4	850	4.9
B	N_6	0.005	6548.4	800	5.0
C	N_4Cl_2	0.112	6548.4	590	5.3
D	N_3O_3	0.070	6548.2	700	6.7
E	N_2O_3S	0.226	6546.5	580	8.6
	N_2O_3[e]	0.089			
F	N_2O_4	0.050	6549.4	710	9.0
G	N_3O_2	0.084	6547.5	600	12.4
H	N_4O_2	0.121	6548.0	560	14.3

[a] Root-mean-square deviation in Mn first coordination sphere distances (Å). [b] Edge energies refer to the energy at the first inflection point of the normalized edge, given in electronvolts. [c] Normalized edge intensities given in squared centimeters per gram. [d] Area for the 1s → 3d region given in electronvolt units × 10^2. [e] Calculated by excluding Mn−S bonds at 2.7 Å. Including just the R < 2.6 Å ligands results in a more accurate representation of the RMS deviation in bond lengths.

EXAFS data reduction followed standard procedures for pre-edge subtraction and spline background removal (Teo, 1986). The pre-edge subtraction and spline data points were nearly identical for all protein and model spectra (see Table S1). The small differences had no effect on the fitting results. Fourier transforms were calculated using weighted data over a range 1.5−11.9 Å^{-1}. EXAFS data were fit over the range 1.5−11.9 Å^{-1}. Initial fits were performed on Fourier-filtered data which was backtransformed over the R range of ca. 1.5−4.7 Å to eliminate high frequency noise. Curve-fitting results to unfiltered data gave equivalent structural results.

Information regarding absorber−scatterer interactions were obtained from fitting the EXAFS data to eq 1,

$$\chi(k) = \sum_s \frac{N_s A_s(k) S}{k R_{as}^2} \exp(-2k^2\sigma_{as}^2)\sin(2kR_{as} + \phi_{as}(k)) \quad (1)$$

where $\chi(k)$ is the fractional modulation in the absorption coefficient above the edge, N_s is the number of scatterers at a distance R_{as}, $A_s(k)$ is the effective backscattering amplitude, S is a scale factor, σ_{as}^2 is the mean-square deviation in R_{as},

ϕ_{as} is the phase shift that the photoelectron wave undergoes in passing through the potentials of the absorbing and scattering atoms, and the sum is taken over all scattering interactions.

Experimental data were simulated using theoretical EXAFS amplitude and phase functions, $A_s(k)$ and $\phi_{as}(k)$,which were calculated using the program FEFF 5.04 (Rehr et al., 1991). Single scattering parameters were calculated for Mn−O, Mn−N, Mn···Mn, and two Mn···C interactions at bond lengths of 2.09, 2.27, 3.60, 3.27, and 4.42 Å, respectively. Multiple scattering parameters were calculated for the 3.27 Å Mn···C_2/C_5 and ca. 4.42 Å Mn···N_3/C_4 interactions found in hexakis−imidazole Mn(II) dichloride. The scale factor, *S*, and threshold energy, E_0, were calibrated by fitting EXAFS data for crystallographically characterized Mn models (Riggs-Gelasco, 1995). A value of 10 eV and a scale factor of 0.9 were found to be the optimum values for all single scattering parameters. Multiple scattering parameters were calibrated by fitting the outer shell EXAFS for hexakis−imidazole Mn(II) dichloride. In this case, the optimum values were 6 eV and $S = 0.75$.

Nonlinear least-squares curve fitting was used to optimize Mn−ligand distances and coordination numbers. In all cases, only *R* and σ were allowed to vary, while the coordination number was held constant and stepped through reasonable values. The weighted root-mean-square deviation between data and fit was calculated as $F = \{[k^6(\text{data} - \text{fit})^2]/N\}^{1/2}$. A more useful statistic is $F' = F^2/\nu$, which accounts for the number of degrees of freedom, ν, given by $\nu = N_{idp} - N_{var}$, where N_{idp} is the number of independent data points, $N_{idp} = (2\Delta k\Delta R)/\pi$, and N_{var} is the number of variables that are refined (Bunker et al., 1991). The $1/\nu$ weighting introduces a penalty for adding additional unnecessary shells of scatterers, and thus provides a more reliable basis for deciding whether an additional ligand interaction is justified (Riggs-Gelasco et al., 1995)

Extended Hückel Calculations. Extended Hückel calculations were performed for all models except **A** and **D** using standard parameters for H, C, N, O, S, and Mn as incorporated in the program CAChe (Oxford Molecular Group). Atoms outside the first coordination sphere were replaced either with protons or, in the case of alkoxides, with methyl groups. The average Mn 4p, Mn 3d, and ligand contributions to the highest occupied molecular orbitals (HOMOs) were determined by summing the relevant orbital contributions from the unoccupied MOs, which showed significant Mn 3d contributions.

RESULTS

XANES Analysis. Normalized XANES spectra are shown in Figure 1. All four edges show a noticeable 1s → 3d peak centered at ca. 6540 eV (inset to Figure 1), followed by an intense absorption edge beginning at ca. 6545 eV. The edge structure for Mn-substituted ribonucleotide reductase and arginase samples is nearly identical, with peak maxima of ca. 800 cm^2/g (see Table 1). In contrast, the edges for Mn-substituted hemerythrin and Mn catalase samples have significantly lower peak maxima of 710 and ca. 660 cm^2/g, respectively. All protein edges are consistent with Mn(II), as shown by representative edges for model complexes **A**, **D**, and **H** (Figure 2). The peak heights for the Mn models

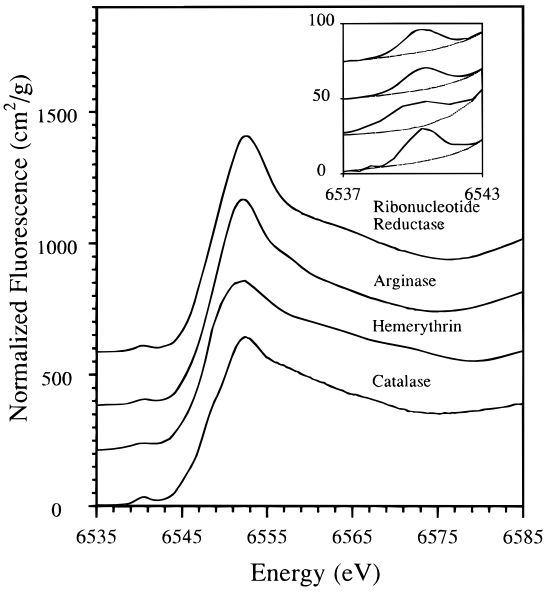

FIGURE 1: Normalized XANES spectra for protein samples. Spectra offset for clarity. (Inset) Region 1s → 3d of the XANES spectra for respective proteins (solid line) with background polynomial (dashed line), plotted in the same order as the full XANES spectra.

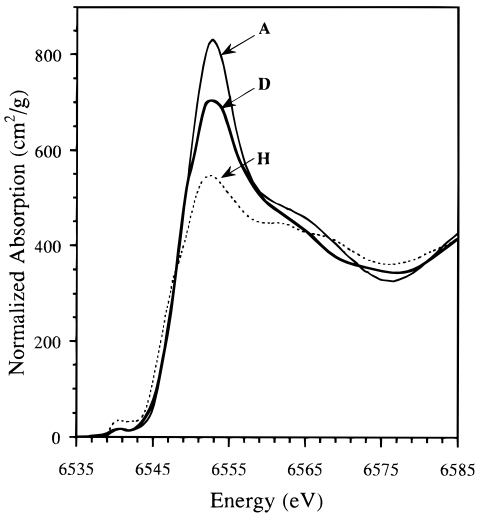

FIGURE 2: Normalized XANES spectra for Mn(II) models $Mn(OH_2)_6^{2+}$ (aq) (**A**), $(pz)_2Mn(OBz)_3Mn(HB(3,5\text{-}iPr_2pz)_3)$ (**D**), and [Mn(2-OH picpn)]$_4$ (**H**).

in Figure 2 range from ca. 850 cm^2/g for the symmetric O_6 model **A** to ca. 560 cm^2/g for the asymmetric N_4O_2 model **H** (see Table 1). In general, the peak height decreases as the nearest neighbor disorder, as judged by the RMS deviation in bond length, increases. The symmetric complexes **A** and **B** both have very intense peak maxima. Complexes **D** and **F**, with mixed N/O ligation have somewhat lower maxima while complex **C**, with mixed N/Cl ligation, and complex **H**, with the largest disorder in Mn−ligand bond length, have the lowest peak maximum. The remaining two complexes, **E** and **G**, have low intensity maxima despite having relatively small bond length disorder. However, these models have either genuine 5-coordinate (**G**) or nearly 5-coordinate (**E**) sites, which may account for their low peak maxima.

First inflection points of the protein XANES spectra range from 6548.0 to 6549.5 eVs, with a standard deviation of ca. 0.3 eV for replicate measurements. These energies are consistent with those for the model compounds. The model

Table 2: Results from Extended Hückel Calculation for Mn(II) Model Complexes with Known Crystal Structures[a]

sample	% Mn 3d	% Mn 4p	% ligand
B	60	0.02	40
C	62	1.0	37
E	51	1.1	48
F	60	1.0	38
G	66	2.6	30
H	63	1.4	36

[a] Crystal structure data for $(pz)_2Mn(OBz)_3Mn(HB(3,5\text{-}iPr_2pz)_3)$ are limited to first coordination sphere distances, so global molecule could not be built for a Hückel calculation.

spectra have edge energies from 6548.0 to 6549.4, with the exception of **E** and **G**. The latter models, with pseudo five-coordinate and true five-coordinate sites, have first inflection points that are 1 eV lower in energy.

The 1s → 3d transition areas for replicate samples were highly reproducible (±0.5), despite the variation in monochromator resolution. The areas for arginase and ribonucleotide reductase were significantly lower than those for Mn catalase and Mn-substituted hemerythrin. The 1s → 3d areas for the models bracket those seen for the proteins. In general, the 1s → 3d area increases with increased bond-length disorder, and is thus negatively correlated with the intensity of the XANES maximum. As expected, the five-coordinate complex, **G**, has one of the highest 1s → 3d intensities (Roe et al., 1984). This intensity is not as high, however, as that seen for the highly disordered six-coordinate complex, **H**. The 1s → 3d areas for ribonucleotide reductase and arginase are similar to those seen for the relatively ordered six-coordinate models, while those for catalase and hemerythrin more closely resemble five-coordinate, or highly disordered six-coordinate models.

Molecular Orbital Calculations. The results of the Hückel calculations are given in Table 2. The calculated percent Mn 4p character is small for all of the models. As expected from simple symmetry considerations, the largest 4p contribution is found for the five-coordinate model, **G**.

Mn−Imidazole EXAFS. The Fourier transform of the EXAFS data for hexakis−imidazole Mn(II) dichloride is given in Figure 3 A. There is an intense Mn−nearest neighbor feature at ca. 2.25 Å ($R + \alpha \approx 1.8$ Å), together with three resolvable features at longer distances. Imidazole EXAFS scattering has been studied extensively, and the importance of multiple scattering from the rigid imidazole ring is well documented (Strange et al., 1986, 1987; Binsted et al., 1993; Wang et al., 1994). Multiple scattering refers to the fact that the X-ray excited photoelectron can be scattered by two (or more) atoms prior to returning to the absorbing atom, as illustrated in Figure 3B. The peak at $R + \alpha \approx 2.6$ Å is due primarily to imidazole C_2/C_5 scattering (see Figure 3B), while those at higher R result primarily from the single and multiple scattering pathways of the imidazole N_3/C_4 atoms. Recently, Wang et al. have described an approach to fitting imidazole scattering in which the imidazole unit is treated as a rigid system (Wang et al., 1994). They found that only in this way was it possible to detect the weak Ni···Ni scattering in urease.

We have adopted a similar approach to analyze the data for model complex **B**. The M−N_1 distance was determined by single scattering EXAFS, and the remaining Mn···(C_2/C_5) and Mn···(N_3/C_4) distances were calculated from the known imidazole ring dimensions (Garrett et al., 1983). Variations of ±5° in the angle between Mn−N_1 and the imidazole plane (ϕ), gave a significant decrease in the apparent distance of the ca. 4.2 Å shell (Figure S1, Supporting Information) that was inconsistent with the data. The value of ϕ was thus set at 0°, in agreement with the crystal structure. The M−N_1−C_5 angle was varied by ±10° around the crystallographic value of 126.3 ° (Figure S2, Supporting Information). The optimum angle was taken as the angle that best reproduced the M···C_2/C_5 feature in the Fourier transform. The best fit was obtained using the crystallographic M−N_1−C_5 angle. These results confirm that properly calibrated FEFF multiple scattering parameters can correctly model imidazole outer shell EXAFS features.

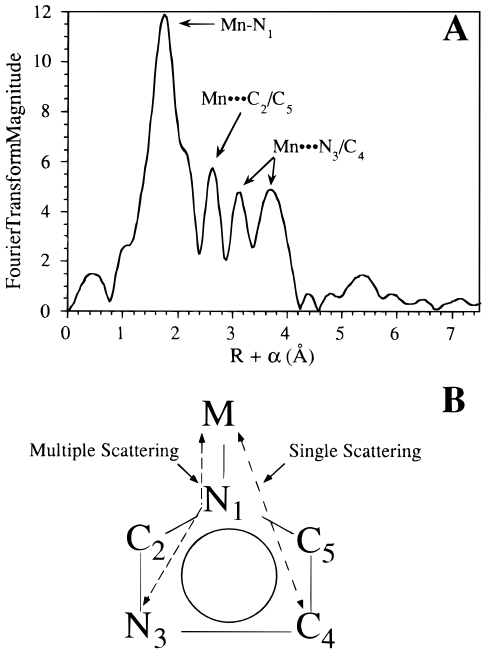

FIGURE 3: Fourier transforms for hexakis−imidazole Mn(II) dichloride with scattering pathways from imidazole structure. (A) Calculated Fourier transform for **B**. (B) Theoretical representation of rigid imidazole structure with single and multiple scattering pathways.

It is essential that the outer shell contributions be modeled correctly, since these can interfere with the detection of metal···metal scattering (Riggs-Gelasco et al., 1995). Thus, the EXAFS data for complex **B** can be fit using either single or multiple scattering theoretical models with nearly equivalent fit quality [see Table 3 and Figure S3 (Supporting Information)]. Fits to the M···C_2/C_5 shell using a single scattering model gave the correct bond length, but underestimated the metal−ligand coordination number. Fits using a multiple scattering model gave correct values for both the bond length and the coordination number. A single scattering model for the 4.42 Å Mn···N_3/C_4 interaction gives the correct coordination number, but a bond length that is off by 0.15 Å. As for the C_2/C_5 shell, fits using multiple scattering models accurately describe both the coordination number and distance of the N_3/C_4 shell. For both single and multiple scattering fits, it is possible to include an additional Mn···Mn shell at a distance that is chemically reasonable for binuclear Mn(II) models. In both cases, the fit quality (F) improves on the addition of Mn···Mn scattering. For the multiple scattering fits, addition of the Mn···Mn shell is not justified, as judged by the slight increase in F'. However, for the

Table 3: EXAFS Fitting Results for Hexakis−Imidazole Mn(II) Dichloride

	Mn − N			Mn ··· C			Mn ··· C/N			Mn ··· Mn			
model type	R^a	CN^b	$\sigma^{2\,c}$	R^a	CN^b	$\sigma^{2\,c}$	R^a	CN^b	$\sigma^{2\,c}$	R^a	CN^b	$\sigma^{2\,c}$	$F'^{\,d}$
single scattering	2.27	5.5	4.1										12.6
	2.27	5.5	4.1	3.28	9.0	5.0							11.0
	2.27	5.5	4.1	3.28	9.0	4.8	4.28	12.0	4.0				7.60
	2.27	5.5	4.2	3.29	9.0	5.5	4.28	12.0	4.0	3.53	0.5	2.4	7.43
multiple scattering	2.27	5.5	4.1										12.6
	2.27	5.5	4.2	3.26	12.0	3.6							9.78
	2.27	5.5	4.2	3.26	12.0	3.5	4.44	12.0	3.8				6.06
	2.27	5.5	4.2	3.20	12.0	7.9	4.44	12.0	4.0	3.25	0.5	0.0	6.14
crystal structure	2.27	6.0		3.27	12.0		4.42	12.0					

[a] Bond length in angstroms. [b] Coordination number giving the best fit. [c] Debye−Waller factor in units of squared angstroms × 10^3. [d] Degrees of freedom weighted goodness of fit (×10^2).

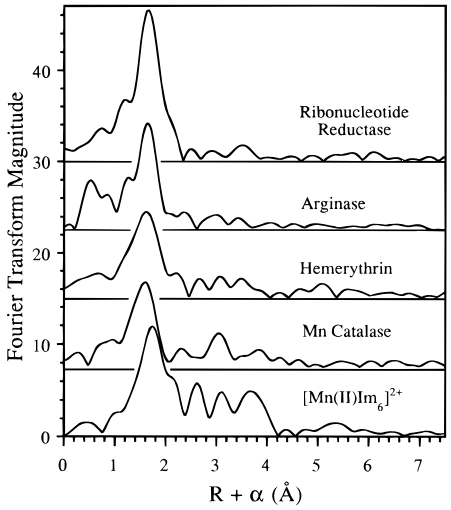

FIGURE 4: Fourier transforms for Mn(II)/Mn(II) proteins and hexakis-imidazole Mn(II) dichloride model. Protein spectra offset for clarity.

single scattering fits there is a slight decrease in *F*′on inclusion of a Mn shell at ca. 3.5 Å which could be misinterpreted as evidence for a Mn···Mn interaction.

Mn(II)/Mn(II) Protein EXAFS. Fourier transforms of the averaged protein EXAFS data are compared to that for complex **B** in Figure 4. The protein spectra all show an intense Mn−nearest neighbor feature at R + α ≈ 1.6 Å, which is ca. 0.15 Å shorter than the Mn nearest neighbor peak for complex **B**. The Mn−nearest neighbor features for ribonucleotide reductase and arginase are narrow and intense, while those for hemerythrin and Mn catalase are broader and less intense. All four protein spectra show weak features in the Mn···C_2/C_5 and Mn···N_3/C_4 scattering regions, although only for hemerythrin do these show good correspondence with the outer shell peaks seen in complex **B**.

Fitting results for the Mn−nearest neighbor interactions are given in Table 4. All four protein spectra can be fit with a single low Z (carbon, oxygen, nitrogen) nearest neighbor shell at average distances which range from 2.12 Å, for Mn catalase, to 2.17 Å for arginase. The single shell fits are characterized by relatively large Debye−Waller factors, indicating disorder in the metal−ligand bond lengths. The apparent coordination numbers are all less than 6. All four protein spectra can be fit with the inclusion of a second low Z shell at a longer distance. However, only in the case of Mn catalase and hemerythrin is inclusion of this second shell justified, based on *F*′, and only in the case of hemerythrin is the improvement in *F*′ dramatic. The distances for the second low Z shell in the catalase and hemerythrin are close to the Mn−N distance in **B**.

Table 4: Mn−Nearest Neighbor EXAFS Fitting Results[a]

	Mn−O			Mn−N			
sample	R^b	CN^c	$\sigma^{2\,d}$	R^b	CN^c	$\sigma^{2\,d}$	F′ ^{e}
Mn_2RR	2.15	5.0	3.7				1.73
	2.07	2.0	2.4	2.18	4.5	1.9	1.91
Arg	2.17	3.5	5.0				1.54
	2.15	3.0	3.2	2.30	1.0	2.0	1.62
Mn_2Hem	2.15	3.0	5.6				4.23
	2.10	3.0	4.3	2.26	2.0	0.3	2.50
Cat	2.12	3.0	5.6				2.76
	2.11	3.0	4.6	2.27	1.0	2.5	2.64

[a] Filtered fits to first shell data (R = 2.0−2.4 Å). Identical results are obtained for fits to unfiltered data. [b] Bond length in angstroms. [c] Best fit coordination number. [d] Debye−Waller factor in units of squared angstroms × 10^3. [e] Degrees of freedom weighed goodness of fit (×10^2)

The nearest neighbor fitting results provide a starting point for defining the outer shell EXAFS (Table 5). In all cases, the data could be fit with Mn···C interactions between ca. 3.0 and 3.6 Å, although in no case was the Mn···C distance uniquely defined. For ribonucleotide reductase, inclusion of a carbon shell between 3.0 and 3.6 Å was not justified, as judged by *F*′. For the other three proteins, the ca. 3 Å carbon shell appears justified. Addition of a second carbon shell at ca. 4.4 Å gave an improvement in *F*′ for arginase, hemerythrin, and Mn catalase. A 4.4 Å carbon shell could also be refined for Mn-substituted ribonucleotide reductase; however, as with the 3 Å carbon shell, this gave a worse fit, as judged by the increase in *F*′.

All four proteins exhibited scattering which could be modeled by a Mn···Mn interaction. However, in every case except Mn catalase, inclusion of a Mn···Mn shell led to an *increase* in *F*′. For ribonucleotide reductase, the apparent Mn···Mn interaction was at 3.30 Å and showed extremely high disorder. The apparent Mn···Mn distance in arginase was slightly longer (3.41 Å) and the Debye−Waller factor for this shell was again larger than the typical values seen in Mn model compounds (Riggs-Gelasco, 1995). Although σ^2 and the Mn···Mn distance (3.50 Å) were reasonable for hemerythrin, the apparent coordination number (0.25) was very low. The increase in *F*′, together with the unreasonable σ^2 or low coordination number, indicates that Mn···Mn scattering does not make a significant contribution to the EXAFS for Mn−ribonucleotide reductase, arginase, and Mn−hemerythrin. In contrast, inclusion of a Mn···Mn shell gave a dramatic decrease in *F*′ for Mn catalase. The best

Table 5: EXAFS Fitting Results for Averaged Dinuclear Mn(II) Protein Data Sets

	Mn−O			Mn−N			Mn···C			Mn···Mn			Mn···C			
sample	R^a	CN^b	$\sigma^{2\,c}$	R^a	CN^b	$\sigma^{2\,c}$	R^a	CN^b	$\sigma^{2\,c}$	R^a	CN^b	$\sigma^{2\,c}$	R^a	CN^b	σ^{2c}	$F'^{\,d}$
Mn_2RR	2.15	5.0	3.7													1.73
	2.15	5.0	3.7				3.02[e]	1.0	11							1.88
	2.15	5.0	3.7										4.42	1.0	2.3	1.85
	2.15	5.0	3.7				3.46[e]	1.0	2.0				4.42	1.0	2.3	2.09
	2.15	5.0	3.7							3.30[g]	0.5	36				1.92
Arg	2.17	3.5	5.0													1.54
	2.17	3.5	5.0				3.07[e]	3.5	4.5							1.21
	2.17	4.0	6.1										4.37	1.0	5.2	1.48
	2.17	4.0	6.1				3.07[e]	4.0	5.3				4.37	1.0	5.0	1.18
	2.17	4.0	6.1							3.41[g]	0.5	10.2				1.40
Mn_2Hem	2.10	3.0	4.3	2.26	2.0	0.3										2.50
	2.10	3.5	5.6	2.26	2.0	0.4	2.98[f]	2.5	3.2							2.38
	2.10	3.5	5.6	2.26	3.0	0.4							4.37	2.5	5.2	2.36
	2.10	3.5	5.6	2.26	2.0	0.4	2.97[f]	2.5	3.2				4.37	2.5	3.9	2.35
	2.10	3.5	5.6	2.26	2.0	0.3				3.50[g]	0.25	4.0				2.59
Cat	2.11	3.0	4.6	2.27	1.0	2.5										2.64
	2.11	3.0	4.6	2.27	1.0	2.6	3.14[e]	3.0	4.2							2.43
	2.11	3.0	4.6	2.27	1.0	2.8							4.42	3.0	0.6	2.46
	2.11	3.0	4.6	2.27	1.0	2.8	3.14[e]	3.0	4.2				4.42	3.0	0.9	2.21
	2.11	3.0	4.5	2.27	1.0	2.2				3.53	0.5	1.6				1.93
	2.11	3.0	4.5	2.27	1.0	1.9	3.09	3.0	3.1	3.54	0.5	1.0	4.41	3.0	0.9	1.33

[a] Bond length in angstroms. [b] Best fit coordination number. [c] Debye−Waller factor in units of squared angstroms × 10^3. [d] Degrees of freedom weighed goodness of fit (×10^2). [e] Alternate minima exist at ca. 3.1 and 3.4 Å. [f] Alternate minima exist at ca. 3.0 and 3.6 Å. [g] Refined Mn···Mn distance does not appear to represent genuine Mn···Mn interaction (see text).

fit was for a coordination number of 0.5; however, the fit was only slightly worse, and the σ^2 slightly larger, if the coordination number was set to 1.0.

The EXAFS fitting properties of Mn catalase are similar to those of binuclear Mn models (Riggs-Gelasco, 1995). In the model compounds[1] , Mn···Mn interactions between 3.2 and 3.8 Å were well modeled by the FEFF-calculated Mn−Mn EXAFS parameters, giving accurate Mn−Mn distances to ±0.02 Å for distances of ca. 3.3 and ±0.05 Å for the longer distances (P. J. Riggs-Gelasco, T. L. Stemmler, A. K. Gelasco, V. L. Pecoraro, and J. E. Penner-Hahn, manuscript in preparation).

Additional fits to the protein EXAFS data were performed in which the distances and coordination numbers for the Mn-N and Mn···C_2/C_5 shells were constrained, based on the observed Mn···N_3/C_4 parameters and the imidazole geometry in **B** (Garrett et al., 1983). In all cases, the constrained fits gave increased F' values. For arginase, hemerythrin, and catalase, the constrained Mn−N interaction had reasonable σ^2 values, while for ribonucleotide reductase, σ^2 for this shell refined to zero. The refined σ^2 values for all of the constrained 3.3 Å Mn···C shells were unusually large in comparison with the model **B**.

The best fits to the unfiltered protein EXAFS gave identical results to those obtained for the filtered spectra. The Fourier transforms of the best fits and the observed data are compared in Figure 5. The unfiltered EXAFS spectra are compared to the best fits in Figure S4 (Supporting Information). The fits are in good agreement with the data, within experimental uncertainty.

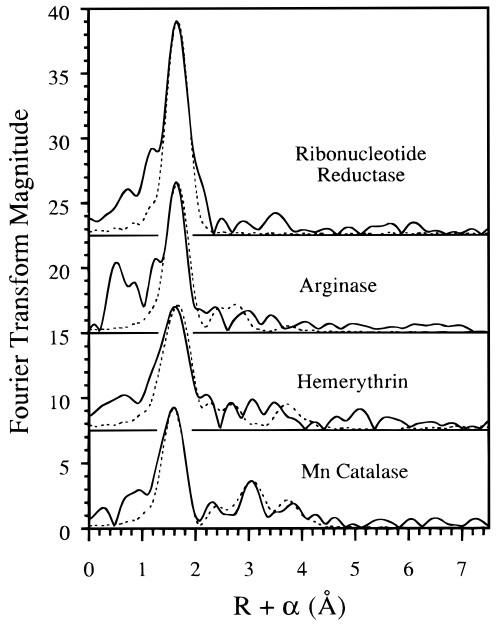

FIGURE 5: Fourier transforms for Mn(II)/Mn(II) proteins (bold) together with the best fit simulated spectra (dashed line).

DISCUSSION

Mn(II) XANES Analysis. The XANES spectra for the model compounds show a clear trend in which the more symmetric models, with smaller deviation in nearest neighbor bond lengths, have the largest peak maxima. The principal absorption minimum can be described as a continuum resonance. The energy of this resonance has been shown to vary approximately as $1/R^2$, where R is the absorber−scatterer distance that gives rise to the continuum resonance (Natoli, 1983; Rehr et al., 1992). It is thus reasonable that an increase in the spread of nearest neighbor bond lengths should result in a decrease in the height of the principal maximum, since each different distance will give rise to a different continuum resonance energy. Only when all of the

[1] Model compounds tested for accuracy of Mn−Mn EXAFS fitting and their Mn−Mn distances include $[Mn^{III}(salpn)(OCH_3)]_2$ (3.194 Å); $TEA_2[Mn^{II}(2\text{-}OH(5\text{-}Clsal)pn]_2$ (3.33 Å); $TEA[Mn^{II}/Mn^{III}$ (2-OH(5-Clsal)pn)$_2$] (3.37 Å); $[Mn^{III}_2(2\text{-}OH(5\text{-}Clsal)pn)_2]$ (3.24 Å); $[Mn^{III}_2(2\text{-}OH(3,5\text{-}Clsal)pn)_2(CH_3OH)]$ (3.81 Å); $(pz)_2Mn(OBz)_3Mn(HB(3,5\text{-}iPr_2pz)_3)$ (3.75 Å) (P. J. Riggs-Gelasco, T. L. Stemmler, A. K. Gelasco, V. L. Pecoraro, and J. E. Penner-Hahn, manuscript in preparation; Riggs-Gelasco, 1995).

Table 6: Comparison of EXAFS Fitting Results with Averaged Crystallographic Parameters

sample		Mn−O		Mn−N		avg Mn−(O/N)[c]		Mn···Mn		number of His residues/Mn
		R^a	CN[b]	R^a	CN[b]	R^a	CN[b]	R^a	CN[b]	
Mn_2RR	(EXAFS)	2.15	5.0			2.15	5.0	nd[f]	nd[f]	nd[f]
	crystal	2.20	3.5	2.25	1.0	2.21	4.5	3.6	1.0	1.0
Arg	(EXAFS)	2.17	3.5			2.17	3.5	3.41	0.5	0.5
	crystal	2.27	4.5	2.15	1.0	2.25	5.5	3.3	1.0	1.0
Mn_2Hem	(EXAFS)	2.10	3.0	2.26	2.0	2.16	5.0	nd[f]	nd[f]	1.0
Fe_2Hem[d]	crystal	2.14	3.0	2.22	2.5	2.18	5.5	3.32	1.0	2.5
Cat	(EXAFS)	2.11	3.0	2.27	1.0	2.15	4.0	3.54	0.5	1.0
	crystal[e]							3.6	1.0	

[a] Bond length in angstroms. [b] Coordination number. [c] Averaged Mn−nearest neighbor distance from all ligands. [d] Coordination information taken from deoxy hemerythrin (Holmes et al., 1991). [e] Only the Mn···Mn separation, determined from a 5.0 Å crystal structure, is presently available. [f] nd = not determined, see text.

energies are nearly identical will a strong absorbance peak be observed. Within this model, it is reasonable that the five-coordinate models (**G** and perhaps **E**) should have lower peak maxima since they have fewer nearest neighbor scatterers. On the basis of the intensity of the principal maximum, arginase and Mn-substituted ribonucleotide reductase have fairly symmetric Mn environments, while Mn catalase and Mn-substituted hemerythrin have significantly less symmetric sites. The decrease in intensities for catalase and hemerythrin could indicate a mixed ligand environment, similar to the N_3O_3 ligation in **D**, or it could reflect a mixture of five- and six-coordinate Mn.

Areas for the 1s → 3d transition typically increase on going from six- to five- to four-coordinate, and this has been used to determine coordination number (Roe et al., 1984; Randall et al., 1993). The basis for the increase in 1s → 3d intensity is the increase in 3d−4p mixing as a metal site goes from octahedral to tetrahedral. The 1s → 3d transition is forbidden by dipole selection rules while the 1s → 4p transition is allowed. Thus, any increase in 4p character will result in an increase in transition intensity. Roe et al. showed a linear correlation between 1s → 3d intensity and 3d + 4p mixing, as judged by extended Hückel calculations (Roe et al., 1984). Qualitatively, we observe similar increases in 1s → 3d intensity as the symmetry decreases, and the five coordinate complex (**G**) has one of the highest 1s → 3d intensities. However, a quantitative comparison of 1s → 3d intensity with 3d + 4p mixing does not show any significant correlation in the present study. Most notably, samples **B** and **C** have dramatically different 4p character in their HOMOs (0.02% vs 1.0%) but nearly identical 1s → 3d intensities. In the case of **G** and **H**, the five-coordinate **G** shows the largest 4p character in its HOMOs, but has a smaller 1s → 3d intensity than **H**. The lack of a correlation between 1s → 3d intensity and 3d + 4p mixing is due, at least in part, to the limited set of models presented in this study, which does not include a wide range of coordination numbers. Nevertheless, it is interesting that the simplistic RMS deviation in bond lengths show a much better correlation with 1s → 3d intensity than does the calculated 3d + 4p mixing for these models.

The structural picture that can be derived from the protein 1s → 3d areas is consistent with that given by the peak maxima. Both arginase and ribonucleotide reductase have weak 1s → 3d transitions, consistent with those seen for the symmetric six-coordinate models. In contrast, Mn-substituted hemerythrin and Mn catalase have significantly more intense 1s → 3d transitions, similar to those seen for the five coordinate or distorted, mixed ligand six-coordinate model complexes. On the basis of both edge shape and 1s → 3d intensity, it appears likely that at least one, and probably both, Mn ions in ribonucleotide reductase and arginase are six coordinate. The crystal structure of Mn-substituted ribonucleotide reductase shows only nine Mn ligands (Atta et al., 1992). The remaining ligands that are suggested by the XANES may be solvent molecules that are either undetected in the crystal structure or absent in the crystalline protein. The XANES data show that the Mn ions in hemerythrin and catalase are either more disordered or have a lower average coordination number, or both. If Mn-substituted hemerythrin had the same structure as ferrous hemerythrin, it would have one six-coordinate site (N_3O_3) and one five-coordinate site (N_2O_3). This would be consistent with the observed XANES, although other possible structures (e.g., two five-coordinate Mn) cannot be ruled out. The XANES data show that Mn catalase has a site that is similar to that in Mn-substituted hemerythrin, although the EXAFS (see below) suggest some differences in ligation.

Nearest Neighbor Ligation. Biochemical and in some cases crystallographic data have shown that all four proteins have both oxygen and nitrogen ligation (Holmes et al., 1991; Atta et al., 1992; Waldo et al., 1992; Cavalli et al., 1994; Ivancich et al., 1995). Despite this mixed ligation, only hemerythrin and catalase showed two resolvable shells of nearest neighbor scatterers. This is not surprising, since the ability to resolve multiple ligand shells depends on the details of the distribution of bond lengths (Riggs-Gelasco et al., 1995). For ribonucleotide reductase, the relatively large apparent coordination number and the small Debye−Waller factor suggests that most of the Mn−ligand bond lengths must be near 2.15 Å. The EXAFS coordination number is substantially larger than the average coordination number of 4.5 seen crystallographically for Mn−ribonucleotide reductase (Table 6). This, together with the relatively ordered site, could be explained by the coordination of several water molecules, in addition to the two carboxylates and the two histidine ligands seen crystallographically. This is thus consistent with the structural properties suggested by the XANES results.

Although the arginase crystal structure shows one five- and one six-coordinate Mn (see Table 6), the arginase EXAFS gives a lower apparent coordination number and a larger Debye−Waller factor than ribonucleotide reductase. This most likely reflects destructive interference between unresolvable scattering interactions in the arginase EXAFS (Baldwin et al., 1994). This could arise either from a

predominantly Mn−O environment with a larger range of Mn-O distances or from a mixture of shorter (Mn−O) and longer (Mn−N) bonds. The outer shell EXAFS (see below) suggests that there are relatively few imidazole ligands in arginase, thus favoring the model in which arginase has a disordered, primarily Mn−O environment. This was confirmed with determination of the crystal structure for arginase (Kanyo et al., 1996). EPR studies have suggested that in the absence of borate, the Mn site in arginase adopts multiple geometries (Khangulov et al., 1995). It is unlikely that this accounts for the observed disorder, as identical EXAFS spectra are seen for native and borate inhibited arginase (T. M. Sossong, Jr., T. L. Stemmler, J. E. Penner-Hahn, and D. E. Ash, unpublished results).

The nearest neighbor environments for Mn-substituted hemerythrin and Mn catalase show evidence for both Mn−O ligands at ca. 2.1 Å and Mn−N ligands at 2.26 Å. These Mn−N distances are typical of those seen for the Mn(II) imidazole structure, and in the case of Mn-substituted hemerythrin, these values closely correlate with those seen in diferrous hemerythrin (Table 6). The apparent Mn−N coordination numbers, one for Mn catalase and two for hemerythrin, suggest that there are two and four His residues, respectively, per Mn_2 core, although this number is not well-defined due to the correlation between the nitrogen and oxygen coordination numbers. This lower limit is in agreement with the five histidine ligands found in the native diiron hemerythrin. The Mn−O shells for both proteins have relatively large Debye−Waller factors, suggesting that there are a range of Mn−O distances.

Mn(II) Imidazole EXAFS. The fitting protocol developed by Wang et al. (1994) does an excellent job of modeling the outer shell imidazole interactions. On the basis of this success, it should be possible to count the number of histidine ligands from analysis of the outer shell EXAFS. An important caveat, however, is that the outer shell EXAFS is quite sensitive to small changes in angle (e.g., Figures S1 and S2, Supporting Information), thus the apparent number of imidazoles is better viewed as an approximate lower limit of the number of histidines. A second important point concerns the apparent presence of Mn···Mn scattering in the mononuclear hexakis−imidazole Mn(II) model. Although Mn···Mn and Mn···C scattering are in principle distinguishable, they can be very difficult to distinguish in practice. With the use of the *F′* statistic and a full multiple scattering treatment of the imidazole scattering, the apparent Mn···Mn shell in the hexakis−imidazole Mn(II) data is seen to be artifactual. Nevertheless, this observation emphasizes the need for caution in interpreting outer shell metal···metal scattering (Riggs-Gelasco et al., 1995).

Although the crystal structure for ribonucleotide reductase shows two Mn−histidine interactions, there is no well-defined Mn···N_3/C_4 shell in the EXAFS for Mn ribonucleotide reductase. This probably reflects disorder in the Mn−imidazole geometries. The other three proteins all show outer shell scattering that can be attributed to a Mn···N_3/C_4 interaction, although this scattering is quite weak in arginase. The amplitude of the Mn···N_3/C_4 shell in Mn hemerythrin is about half of that expected based on the crystal structure of ferrous hemerythrin. As with ribonucleotide reductase, this probably reflects orientational disorder of the imidazoles.

None of the proteins give Mn···C_2/C_5 distances that are consistent with the observed Mn···N_3/C_4 distances or with the expected Mn(II)−imidazole structure. The Mn···C_2/C_5 distances should be ca. 3.3 Å, but they consistently refine to either shorter or longer distances. This must reflect the presence of additional scattering atoms at similar distances. One possible scatterer in the range of 3.0 Å < R < 3.5 Å is Mn, and indeed, the scattering between 3.0 and 3.5 Å could always be fit by including a Mn···Mn interaction. However, only for catalase did the Mn···Mn shell give a better fit (*F′*) with a reasonable coordination number and Debye−Waller factor. For the other three proteins, the Mn···Mn shell behaved similarly to the Mn···Mn shell used to fit model **B** (Table 3). Thus, the "Mn···Mn" shell for ribonucleotide reductase, arginase, and hemerythrin most likely reflects an unsuccessful attempt to mimic Mn···C EXAFS with a Mn···Mn interaction.

The other candidate for the source of additional scattering between 3.0 and 3.5 Å is carboxylate carbons (Riggs-Gelasco, 1995). There is relatively little previous evidence for significant contributions of carboxylate carbons to outer shell EXAFS. However, bridging or bidentate carboxylates should be sufficiently rigid to make detectable contributions in this region. We therefore attribute the Mn···C shell at ca. 3.0 Å to a mixture of Mn···C_2/C_5 scattering at ca. 3.3 Å and Mn···carboxylate scattering at other distances. It is noteworthy that attempts to fit the data with rigid imidazole ligands (i.e., with constrained Mn-N_1 and Mn···C_2/C_5 shells) do *not* give improved fits. This may be a general property of proteins that have a significant number of both histidine and carboxylate ligands. Even though a Mn···C shell must be present at ca. 3.3 Å, particularly for Mn hemerythrin, this shell is not independently resolvable.

The structural picture which emerges from consideration of both the first shell and outer shell EXAFS is one in which catalase and hemerythrin have the largest fraction of histidine ligands. This is consistent with the crystal structures of arginase and Mn-substituted ribonucleotide reductase and with the expected structure of hemerythrin (Holmes et al., 1991; Atta et al., 1992; Kanyo et al., 1996). For catalase, where high-resolution crystal structures are not yet available, the EXAFS data suggest a lower limit of two His ligands per binuclear site. If there are only two, then they must be more ordered than the two His ligands in arginase and Mn−ribonucleotide reductase.

Only Mn catalase shows clear evidence for an EXAFS detectable Mn···Mn shell. The absence of a Mn···Mn shell in Mn-substituted ribonucleotide reductase is somewhat surprising, since the crystal structure shows a 3.6 Å Mn···Mn distance. We attribute the absence of Mn···Mn EXAFS to the fact that the Mn are bridged only by carboxylate bridges (Atta et al., 1992). In the absence of a single atom bridge (oxo, hydroxo, or aquo), Mn···Mn EXAFS is unlikely to be readily detectable (Riggs-Gelasco et al., 1995).

The absence of detectable Mn···Mn EXAFS for arginase is even more surprising given the crystallographic evidence for two single atom bridges (see Scheme 1) and the relatively short ∼3.3 Å Mn···Mn distance. A likely explanation is that, at the pH of the EXAFS measurements, the hydroxide bridge seen in the crystal structure (pH ≈ 8.5) (Kanyo et al., 1992) is protonated (Kuhn et al., 1991). This would result in either the loss or the weakening of the bridge and would explain the lack of detectable Mn···Mn EXAFS. EPR measurements have shown the coupling between the Mn atoms in arginase is ca. 4-fold weaker than that in Mn

catalase (Khangulov et al., 1995). The weak coupling in arginase was interpreted as evidence for an aqua bridge. However, the magnitude of the exchange interaction is also consistent with the presence of only carboxylate bridges. The EXAFS data are consistent with either structure.

Although diferrous hemerythrin has a hydroxide bridge between the irons, it is not known what, if any, bridging ligands are present for Mn hemerythrin (Holmes et al., 1991). The observation of a six-line EPR signal for Mn hemerythrin (Zhang, 1992) indicates the lack of significant coupling between the Mn, thus suggesting that there are either no bridging ligands, or possibly only carboxylate bridges. The absence of a single atom bridge would explain the lack of detectable Mn···Mn EXAFS in Mn hemerythrin.

The observation of Mn···Mn EXAFS only for Mn catalase suggests that Mn catalase has a unique binuclear structure in comparison with the other three proteins. The EXAFS Mn···Mn distance is in good agreement with the low resolution crystal structure and with the Mn···Mn distance deduced by Khangulov et al. (1995) from EPR data for the *T. thermophilus* enzyme (Vainshtein et al., 1984; Baldwin, 1990). More recently, Meier et al. (1996) have reported EPR data for the *L. plantarum* Mn catalase. These showed approximately 2-fold stronger antiferromagnetic coupling than was seen for the *T. thermophilus* enzyme. The *L. plantarum* EPR data were interpreted as evidence for a Mn(μ-OH)$_2$Mn core structure. The 3.53 Å EXAFS Mn···Mn distance is too long to be consistent with a di-μ-hydroxo-bridged structure in our samples, since the di-μ-hydroxo bridged structure would have a Mn···Mn distance of 3.3 Å (Kitajima et al., 1991). The weaker coupling in the *T. thermophilus* enzyme was interpreted as evidence for a hydroxo-, carboxylato-bridged binuclear core. The EXAFS data are consistent with this model. It appears that at least one single-atom bridge is necessary to observe EXAFS detectable metal···metal scattering, and there is ample evidence that a μ-OH ligand can fulfill this role (Riggs-Gelasco et al., 1995). The observed Mn···Mn distance is somewhat longer than those typically seen for hydroxo-, carboxylato-bridged dimers (typically 3.3 Å) and is more representative of the Mn···Mn distances found for aquo-, carboxylato-bridged complexes (ca. 3.6 Å) (Bossek & Wieghardt, 1989; Caneschi et al., 1989; Yu et al., 1992). Although the range of Mn···Mn distances that are seen crystallographically is sufficiently large that the 3.6 Å EXAFS distance cannot be used to distinguish between μ-hydroxo and μ-aquo ligation, the 3.6 Å distance does suggest that μ-aquo ligation should be considered for the Mn catalase.

There appears to be no clear answer regarding the detectability of metal···metal EXAFS in aquo-, carboxylato-bridged binuclear sites. An Fe···Fe interaction is not seen for reduced methane monooxygenase (MMO), whose di-iron(II) site shows bidentate and monodentate carboxylate bridges and a semibridging aqua ligand with an Fe···Fe distance of 3.28 Å (DeWitt et al., 1991). This may indicate that μ-aquo bridges are too disordered to give detectable metal···metal EXAFS, or may be a result that is idiosyncratic to MMO.

The exchange coupling for Mn catalase is somewhat larger than the values typically found for μ-aquo-bridged Mn dimers (Khangulov et al., 1995). However, as with bond lengths, the range of observed values is too large to permit unambiguous discrimination between the μ-hydroxo and μ-aquo ligation. We tentatively favor the (aquo, carboxylato)-bridged model for Mn catalase on the basis of the relatively long Mn···Mn distance. This model leads to the prediction that the smaller exchange coupling for arginase relative to catalase is a consequence of loss of a bridging water, rather than the protonation of a bridging hydroxide (Khangulov et al., 1995). This would explain how the Mn ions in arginase could fail to give rise to EXAFS detectable Mn···Mn scattering, despite both crystallographic (Kanyo et al., 1996) and EPR (Khangulov et al., 1995) evidence that they are in close proximity. A revised proposal for the Mn catalase active site, based on these assumptions, is shown in Figure 6. In this, one Mn is drawn five-coordinate and one six-coordinate, to account for the 1s → 3d area, and to provide a vacant coordination site at which H_2O_2 might bind. On the basis of the outer shell EXAFS, two to three histidine ligands are probably present; however, their relative placement is unknown. Although EXAFS provides no evidence for the number of carboxylate bridges, two are drawn based on the ligation seen in many other binuclear Fe and Mn proteins. Two bridging carboxylates would help to make the Mn···Mn EXAFS signal detectable.

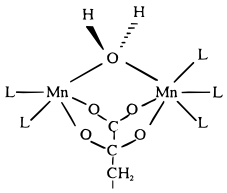

FIGURE 6: Possible structure for the Mn(II)/Mn(II) catalase. L = histidine, carboxylate or solvent ligands.

Catalase Reactivity. The H_2O_2 disproportionation activity of arginase and Mn-substituted ribonucleotide reductase is 1000-fold lower than that of Mn catalase, while Mn hemerythrin shows no detectable reaction with hydrogen peroxide (T. E. Elgren, unpublished results; Zhang, 1992; Shank et al., 1994; Sossong et al., 1997). It is intriguing that arginase and Mn-substituted ribonucleotide reductase have very similar structures, as judged by EXAFS, and are structurally distinct from the other two proteins. On the basis of their EXAFS spectra, arginase and Mn-substituted ribonucleotide reductase both appear to have very symmetric, approximately six-coordinate, ligation spheres. One possible explanation for their low catalytic activity is thus their lack of a vacant or readily exchangeable site for substrate binding. Alternatively, the lack of a detectable Mn···Mn interaction in arginase and ribonucleotide reductase may reflect loss of a catalytically important bridging ligand (either aquo or hydroxo). On the basis of the XANES, Mn-substituted hemerythrin appears likely to have at least one five-coordinate Mn which could serve as a binding site for hydrogen peroxide. It is not clear why this protein is catalytically inactive. One possibility is the larger number of histidine ligands that appear to be coordinated to the Mn atoms in Mn hemerythrin. These would be expected to stabilize the Mn(II)/Mn(II) oxidation state, thereby inhibiting facile oxidation to the Mn(III)/Mn(III) level. Also, constraints from the surrounding protein may render the dimetal site in hemerythrin coordinatively less flexible, thus creating a barrier to oxidation state changes which is not present in the other proteins. Such a barrier may, in fact, be crucial for reversible O_2 binding, which is hemerythrin's biological

function (Stenkamp, 1994). In contrast, the diiron site in ribonucleotide reductase undergoes substantial structural rearrangement upon oxidation state changes (Nordlund & Eklund, 1995). Alternatively, the lack of exchange coupling between the two Mn in hemerythrin may indicate the absence of bridging ligands. Mn catalase evidently has a site which is tailored to avoid the limitations that are present in these other proteins. Future studies, particularly in mutant proteins, may shed light on which structural features are essential to catalysis.

ACKNOWLEDGMENT

We thank the Pecoraro, Kitajima, and Goff groups for model compound preparation and Ji-Hu Zhang for preparation of manganese-substituted hemerythrin.

SUPPORTING INFORMATION AVAILABLE

Figures showing dependence of FT for Mn(II)hexakisimidazole on ϕ (Figure S1) and comparing theoretical and empirical data for this model (Figures S2 and S3); unfiltered EXAFS data and the best fits for all four proteins (Figure S4); and the EXAFS data collection and reduction parameters (Table S1) (5 pages). Ordering information is given on any current masthead page.

REFERENCES

Atkin, C., Thelander, L., Reichard, P., & Lang, G. (1973) *J. Biol. Chem. 248,* 7464−7472.
Atta, M., Nordlund, P., Aaberg, A., Eklund, H., & Fontecave, M. (1992) *J. Biol. Chem. 267,* 20682−20688.
Baldwin, E. (1990) Ph.D. Thesis, University of North Carolina, Chapel Hill.
Baldwin, M. J., Stemmler, T. L., Riggs-Gelasco, P. J., Kirk, M. L., Penner-Hahn, J. E., & Pecoraro, V. L. (1994) *J. Am. Chem. Soc. 116,* 11349−11356.
Barynin, V. V., & Grebenko, A. I. (1986) *Dokl. Acad. Nauk SSSR 286,* 461−464.
Beyer, W. F. J., & Fridovich, I. (1985) *Biochemistry 24,* 6460−6467.
Binsted, N., Strange, R. W., & Hasnain, S. S. (1993) *Jpn. J. Appl. Phys. 32-2,* 141−143.
Bossek, U., & Wieghardt, K. (1989) *Inorg. Chim. Acta* 123−129.
Bunker, G., Hasnain, S., & Sayers, D. (1991) in *X-ray Absorption Fine Structure* (S. S. Hasnain, Ed.) Ellis Horwood, New York, 751−770.
Caneschi, A., Ferraro, F., Gatteschi, D., Melandri, M. C., Rey, P., & Sessoli, R. (1989) *Angew. Chem 101,* 1408−1409.
Cavalli, R. C., Burke, C. J., Kawamoto, S., Soprano, D. R., & Ash, D. E. (1994) *Biochemistry 33,* 10652−10657.
DeWitt, J. G., Bentsen, J. G., Rosenzweig, A. C., Hedman, B., Green, J., Pilkington, S., Papaefthymiou, G. C., Dalton, H., Hodgson, K. O., & Lippard, S. J. (1991) *J. Am. Chem. Soc. 113,* 9219−9235.
Fronko, R. M., Penner-Hahn, J. E., & Bender, C. J. (1988) *J. Am. Chem. Soc. 110,* 7554−7555.
Gamelin, D. R., Kirk, M. L., Stemmler, T. L., Pal, S., Armstrong, W. H., Penner-Hahn, J. E., & Solomon, E. I. (1994) *J. Am. Chem. Soc. 116,* 2392−9399.
Garrett, T. P. J., Guss, J. M., & Freeman, H. C. (1983) *Acta. Crystallogr. C39,* 1027−1031.
Gelasco, A., Askenas, A., & Pecoraro, V. L. (1996) *Inorg. Chem. 35,* 1419−1420.
Gelasco, A. K. (1995) Ph.D. Thesis, The University of Michigan.
Greenberg, D. M. (1960) in *The Enzymes* (Boyer, P. D., Lardy, H., and Myrback, K., Eds.) 2nd ed., Vol. 4, pp 257−267, Academic Press, New York.
Grush, M. M., Chen, J., Stemmler, T. L., George, S. J., Ralston, C. Y., Stibrany, R. T., Gelasco, A., Christou, G., Gorun, S. M., Penner-Hahn, J. E., et al. (1996) *J. Am. Chem. Soc. 118,* 65−69.
Hertzfeld, A., & Raper, S. M. (1976) *J. Biochem. 153,* 469−478.
Holmes, M. A., Le, T. I., Turley, S., Sieker, L. C., & Stenkamp, R. E. (1991) *J. Mol. Biol. 218,* 583−593.
Ivancich, A., Barynin, V. V., & Zimmermann, J. L. (1995) *Biochemistry 34,* 6628−6639.
Kang, J. H., & Cho, Y. D. (1990) *Plant Physiol. 93,* 1230−1234.
Kanyo, Z., Scolnick, L. R., Ash, D. E., & Christianson, D. W. (1996) *Nature 383,* 554−557.
Kanyo, Z. F., Chen, C.-Y., Daghigh, F., Ash, D. E., & Christianson, D. W. (1992) *J. Mol. Biol. 224,* 1175−1177.
Kessissoglou, D. P., Butler, W. M., & Pecoraro, V. L. (1987) *Inorg. Chem. 26,* 495−503.
Khangulov, S., Sivaraja, M., Barynin, V. V., & Dismukes, G. C. (1993) *Biochemistry 32,* 4912−4924.
Khangulov, S. V., Barynin, N. V., Melik-Adamyan, V. R., Grebenko, A. I., & Ilysova, U. B. (1986) *Bioorg. Xhim. 12,* 741−748.
Khangulov, S. V., Pessiki, P. J., Barynin, V. V., Ash, D. E., & Dismukes, G. C. (1995) *Biochemistry 34,* 2015−2025.
Kitajima, N., Sihgh, U. P., Amagai, H., Osawa, M., & Moro-oka, Y. (1991) *J. Am. Chem. Soc. 113,* 7757−7758.
Kono, Y., & Fridovich, I. (1983) *J. Biol. Chem. 258,* 6015−6019.
Kuhn, N. J., Talbot, J., & Ward, S. (1991) *Arch. Biochem. Biophys. 286,* 217−221.
Kurtz, D. M. J., Shriver, D. F., & Klotz, I. M. (1977) *Coord. Chem. Rev. 20,* 39−51.
Lynch, J. B., Juarez-Garcia, C., Münck, E., & Que, L., Jr. (1989) *J. Biol. Chem. 264,* 8091−8096.
McMaster, W. H., Del Grande, N. K., Mallett, J. H., & Hubbel, J. H. (1969) Compilation of X-Ray Cross Sections, U.S. Department of Commerce, UCRL-50174-SEC 2-R1.
Meier, A. E., Whittaker, M. M., & Whittaker, J. W. (1996) *Biochemistry 35,* 348−360.
Natoli, C. R. (1983) in *Springer Series in Chemical Physics* (Bianconi, A., Incoccia, L., and Stipcich, S., Eds.) Springer-Verlag, Berlin, 43−56.
Nordlund, P., & Eklund, H. (1993) *J. Mol. Biol. 232,* 123−164.
Nordlund, P., & Eklund, H. (1995) *Curr. Opin. Struct. Biol. 5,* 758−766.
Nordlund, P., Sjöberg, B.-M., & Eklund, H. (1990) *Nature 345,* 593−598.
Petersson, L., Graeslund, A., Ehrenberg, A., Sjoeberg, B. M., & Reichard, P. (1980) *J. Biol. Chem. 255,* 6706−6712.
Que, L. J., & True, A. E. (1990) in *Prog. Inorg. Chem.* (Lippard, S. J., Ed.) John Wiley & Sons, New York, 97−200.
Randall, C. R., Zang, Y., True, A. E., Que, L. J., Charnock, J. M., Garner, C. D., Fujishima, Y., Schofield, C. J., & Baldwin, J. E. (1993) *Biochemistry 32,* 6664−6673.
Reczkowski, R. S., & Ash, D. E. (1992) *J. Am. Chem. Soc. 114,* 10992−10994.
Rehr, J. J., Mustre, D. L. J., Zabinsky, S. I., & Albers, R. C. (1991) *J. Am. Chem. Soc. 113,* 5135−5140.
Rehr, J. J., Albers, R. C., & Zabinsky, S. I. (1992) *Phys. Rev. Lett. 69,* 3397−3400.
Riggs-Gelasco, P. J. (1995) Ph.D. Thesis, The University of Michigan.
Riggs-Gelasco, P. J., Stemmler, T. L., & Penner-Hahn, J. E. (1995) *Coord. Chem. Rev. 144,* 245−286.
Roe, A. L., Schneider, D. J., Mayer, R. J., Pyrz, J. W., Wisdom, J., & Que, J. L. (1984) *J. Am. Chem. Soc. 106,* 1676−1681.
Salowe, S., & Stubbe, J. (1986) *J. Bacteriol. 165,* 363−366.
Salowe, S. P. (1987) Ph.D. Thesis, University of Wisconsin, Madison.
Shank, M., Barynin, V., & Dismukes, G. C. (1994) *Biochemistry 33,* 15433−15436.
Sossong, T. M., Jr., Khangulov, S. V., Cavalli, R. C., Soprano, D. R., Dismukes, G. C., & Ash, D. E. (1997) *J. Biol. Inorg. Chem.* (in press).
Stemmler, T. L. (1996) Ph.D. Thesis, The University of Michigan.
Stenkamp, R. E. (1994) *Chem. Rev. 94,* 715−726.

Strange, R. W., Hasnain, S. S., Blackburn, N. J., & Knowles, P. F. (1986) *J. Phys., Colloq. 47,* C8/593−C8/596.
Strange, R. W., Blackburn, N. J., Knowles, P. F., & Hasnain, S. S. (1987) *J. Am. Chem. Soc. 109,* 7157−7162.
Stubbe, J., & van der Donk, W. A. (1995) *Chem. Biol. 2,* 793−801.
Teo, B. K. (1986) *EXAFS: Basic Principles and Data Analysis,* New York, Springer-Verlag.
Vainshtein, B. K., Melik-Adamyan, W. R., Barynin, V. V., & Vagin, A. A. (1984) in *Progress in Bioorganic Chemistry and Molecular Biology* (Ovchinnikov, Y., Ed.) Elsevier, Amsterdam, New York and Oxford, 117-132.
Waldo, G. S. (1991) Ph.D. Thesis, The University of Michigan.
Waldo, G. S., & Penner-Hahn, J. E. (1995) *Biochemistry 34,* 1507−1512.
Waldo, G. S., Fronko, R. M., & Penner-Hahn, J. E. (1991) *Biochemistry 30,* 10486−10490.
Waldo, G. S., Yu, S., & Penner-Hahn, J. E. (1992) *J. Am. Chem. Soc. 114,* 5869−5870.
Wang, S., Lee, M. H., Hausinger, R. P., Clark, P. A., Wilcox, D. E., & Scott, R. A. (1994) *Inorg. Chem. 33,* 1589−1593.
Yu, S. B., Lippard, S. J., Shweky, I., & Bino, A. (1992) *Inorg. Chem. 31,* 3502−3504.
Zhang, J.-H. (1992) Ph.D. Thesis, University of Georgia.
Zhang, J. H., & Kurtz, D. M. J. (1992) *Proc. Natl. Acad. Sci. U.S.A. 89,* 7065−7069.
Zhang, J. H., Kurtz, D. M. J., Maroney, M. J., & Whitehead, J. P. (1992) *Inorg. Chem. 31,* 1359−1366.

BI9702795